Reprogrammable 3D Shaping from Phase Change Microstructures in Elastic Composites

Heng Deng<sup>1#</sup>, Xianchen Xu<sup>1#</sup>, Cheng Zhang<sup>1</sup>, Jheng-Wun Su<sup>1</sup>, Guoliang Huang<sup>1\*</sup>, Jian Lin<sup>1,2,3\*</sup>

<sup>1</sup>Department of Mechanical and Aerospace Engineering

<sup>2</sup>Department of Electrical Engineering and Computer Science

<sup>3</sup>Department of Physics and Astronomy

University of Missouri, Columbia, Missouri 65211, USA.

Emails: linjian@missouri.edu or huangg@missouri.edu

# These authors contributed equally to this work

**ABSTRACT** 

Herein, we demonstrate reprogrammable 3D structures that assemble from elastic composite

sheets made from elastic materials and phase change microparticles. By controlling the phase

change of the microparticles by localized thermal patterning, anisotropic residual strain is

generated in the pre-stretched composite sheets, and then triggers 3D structure assembly when the

composite sheets are released from the external stress. Modulation of the geometries and location

of the thermal patterns leads to complex 2D-3D shaping behaviors such as bending, folding,

buckling and wrinkling. Due to the reversible phase change of the microparticles, these

programmed 3D structures can later be recovered to 2D sheets once they are heated for

reprogramming different 3D structures. To predict the 3D structures assembled from the 2D

composite sheets, finite element modeling was employed, which showed reasonable agreement

with the experiments. The demonstrated strategy of reversibly programming 3D shapes by

controlling phase change microstructures in the elastic composites offers unique capabilities in

fabricating functional devices such as a rewritable "paper" and a shape reconfigurable pneumatic

actuator.

**KEYWORDS:** 3D structures, assembly, phase change, reprogrammable materials, composites

1

## **INTRODUCTION**

Three-dimensional (3D) structures are crucial for materials to rationally tailor their properties for applications in tissue engineering, optics and electronics, robotics, energy storage and so forth.<sup>1-7</sup> There are several traditional techniques to fabricate 3D structures such as molding, engraving, and additive manufacturing. 8 However, cost and time consumed by using these direct fabrication methods often increase rapidly with shape complexity. Compared to the direct 3D fabrication, planar fabrication techniques are inexpensive and have high throughput. It has become of strategic significance to employ planar fabrication to make 2D-formed materials or devices and then assemble them to complex 3D structures in different length scales. A recently demonstrated mechanically guided assembly of 2D membranes to 3D architectures has shown such a new frontier. This assembly method is applicable across material classes ranging from flexible polymers to brittle inorganics, and can realize 3D structures in length scales from tens of nanometers to centimeters. 9-12 The resulting 3D structures have shown applications in wearable electronics, <sup>13</sup> 3D photodetection, <sup>14</sup> energy storage, <sup>15</sup> microrobotics, <sup>16</sup> and biomedical devices. <sup>17</sup> However, it involves multiple processing steps, requiring high-cost masks, restricted alignment, transfer printing, and tedious post-processing. 12 Second, the resulting 3D structures are not freestanding because they are locked onto planar elastomeric substrates. To make them free-standing, extra processing and materials are needed. 18

Another strategy of forming 3D structures is to utilize shape programmable materials, which are often stimuli-responsive polymers, hydrogels, and organogels. These materials can transform their shapes from planar sheets to 3D architectures upon external stimuli.<sup>5, 19</sup> The shape-morphing behaviors are often determined by spatially controlled anisotropic domains, which can be generated by techniques such as photolithography, <sup>20-21</sup> ion printing, <sup>22</sup> 4D printing, <sup>23-24</sup> magnetic

patterning, <sup>25-26</sup> and direct laser writing (DLW). <sup>27-30</sup> Upon stimuli, the spatial anisotropies of the materials give rise to non-uniform volume change that induces the in-plane or/and out-of-plane shape transformation. Even though a series of complex 3D structures have been realized through bending, folding, buckling, and wrinkling of these responsive materials, their drawbacks are obvious. First, the self-morphed 3D structures can only be maintained unless the stimuli are kept. Second, the anisotropies created in these materials are often determined permanently, thus the final resulting 3D structures are fixed. However, in many practical applications, reprogramming the 3D structures upon demanded is highly desired.

Shape memory polymers (SMPs) can be reprogrammed to different geometries. Their temporary 3D shapes are first fixed and subsequently recover to their permanent and programmed shapes upon stimulation (typically heat). These temporary 3D shapes are very stable as long as the temperature is below the transition temperature (T<sub>tran</sub>). In addition, the programmed shapes can be erased and re-encoded, thus diverse 3D structures can be reprogrammed from the same materials. Despite these advantages, the biggest challenge of using SMPs to fabricate 3D structures is that in order to achieve complex 3D geometries spatially resolved mechanical force needs to be applied for shape programming. Although other planar chemical patterning techniques such as deprotonation and transesterification were employed to create domains with anisotropic properties in the SMP sheets, restricted reactions involving strong alkali or toxic organic solvent were needed. In addition, the resulting 3D structures are static once patterned, showing no further shape reconfiguration capability.

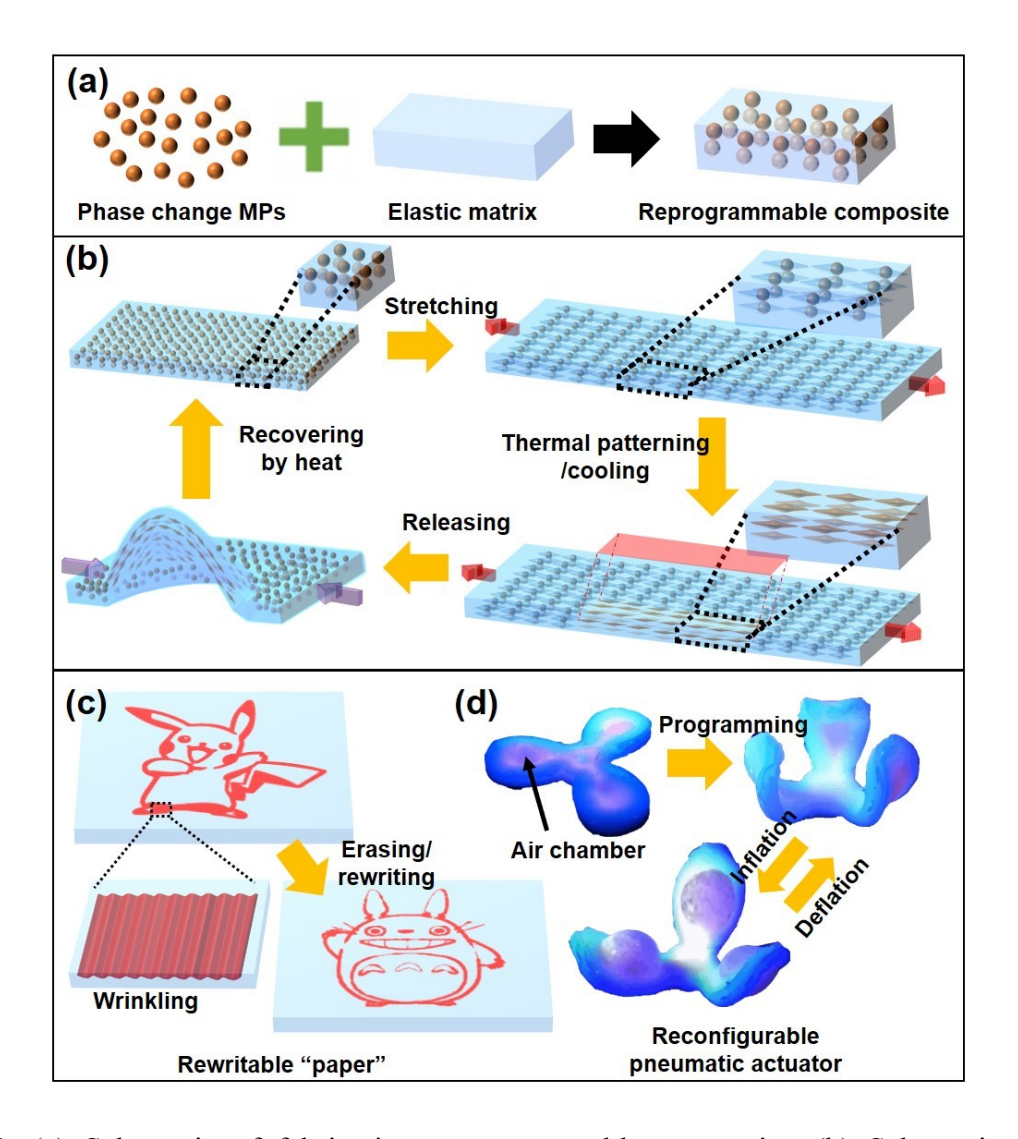


**Figure 1.** (a) Schematic of fabricating reprogrammable composite. (b) Schematic of shape programming and reprogramming process of the composite sheets. Applications of reprogrammable composite as a rewritable "paper" (c) and a reconfigurable pneumatic actuator (d).

Herein, we report a reprogrammable elastic composite (Figure 1a) that can achieve reprogrammable 2D-to-3D shape transformations by a simple thermal patterning process (Figure 1b). The reprogrammable elastic composites were fabricated by embedding phase change microparticles (MPs) such as wax MPs or polycaprolactone (PCL) MPs into elastic matrix such as silicone elastomer or hydrogel. Their reprogrammable shape-morphing functions were endowed from the embedded phase change MPs with a phase change property between solid and liquid.

Compared to ordinary SMPs whose shape memory effect arises from the reconfiguration of polymer chains, the demonstrated reprogrammable composite sheet shows the shape memory effect because of its constituent components. This novel mechanism allows a simple thermal patterning to be applied to program the 3D shapes. In brief, upon heating the phase change MPs undergo the phase change from solid to liquid so that their morphology is changed to micro spindle shape when the melted MPs adapts to the geometry of the cavity that is formed in the elastic materials upon stretching. After cooled down, these thermally exposed regions with the solid micro spindles exhibit residual strain after the pre-stretched composite sheets are relaxed by removing the applied stress. Thus, the thermally exposed regions shrink less volume than the non-exposed ones, leading to internal stress between them, which triggers the in-plane buckling action or outof-plane folding/bending to form 3D shapes (Figure 1b). If the formed 3D structures are globally heated, the phase change of the MPs from solid to liquid releases the residual strain, thus making the 3D structures recover to the 2D sheets that can be reprogramed to different 3D structures by the same method. Based on this phase change composite, complex 3D shape transformations such as bending, folding and buckling were achieved. In addition, by adopting direct CO2 laser patterning, wrinkle structures can be repeatedly written and erased on the surface of an elastic composite, behaving like a rewritable "paper" (Figure 1c). Finally, due to a large elasticity of the composite, a soft pneumatic actuator was fabricated (Figure 1d). The 3D shaped actuator was first transformed from a thermally patterned 2D composite sheet and then showed shape reconfiguration by air inflation. With different thermal patterns, different motions, e.g. individual or cooperative grabbing actuation, were realized in the same device.

#### RESULTS AND DISCUSSION

To conceptually verify this idea, we firstly used commercial wax and silicone elastomer to fabricate the reprogrammable composite sheet. The fabrication process of Wax-silicon (W-silicone) composite sheets is schematically represented in Figure 2a and described in the experimental section. In brief, the wax was melted and thoroughly mixed with commercial silicone elastomer solution (Ecoflex 00-30) followed by curing at room temperature. To fabricate a series of Wsilicone composites, the mass ratios of the wax were varied from 20 wt% to 60 wt%. Due to phase separation, <sup>36</sup> the wax was physically mixed with the silicone and formed MPs. To investigate the 3D shaping mechanism, we first studied the origin of the residual strain. To do that, the W-silicone strips were stretched to a strain of 100% in the uniaxial direction. Then the stretched W-silicone strips were heated at 100 °C to melt the wax MPs followed by cooling to room temperature. Distinguished from pure silicone elastomer strips which were fully recovered to original shapes, the W-silicone strips showed the residual strain after the applied external stress was removed (Figure S1). The residual strain is characterized by  $(L_f-L_0)/L_0$ , where  $L_f$  is the final length of the strip after a strip is relaxed, and L<sub>0</sub> is the original length of a strip (Figure 2b). Further characterization shows that the residual strain depends on the mass ratio of the wax. It increases from 40% to 76% as the mass ratio of the wax increases from 20 wt% to 60 wt%. Creation of spatially distributed residual strain can lead to 2D-to-3D shape transformations as reported in our previous work.<sup>37</sup> However, the residual strain was permanently locked, leading to no shape reprogramming capability. In contrast, in the current work, the residual strain is erasable by heat for reversible shape programming. It should be noted that the wax also affects the elasticity of the W-silicone composites. As shown in Figure 2c, no obvious plastic deformation is observed in the of W-silicone strips that have the wax with a mass ratio of up to 30 wt%, while the W-silicone

strips with 60 wt% wax show 10.6% residual strain even though they are not thermally patterned. To better program 3D shapes, it is better that the thermally exposed regions in the W-silicone sheets possess high residual strain while no or little residual strain is induced in the non-exposed regions. To balance them, the W-silicone composites with 30 wt% wax were chosen for the following shape-morphing experiments. To investigate reversibility and stability of shape-morphing behaviors of W-silicone composites, cycling test of the residual strain in a W-silicone composite sheet was also conducted. During 100 cycles of shape programming process stretching, heating, cooling, and releasing (Figure S2a), the residual strain in a W-silicone composite is consistent and can be erased by heat (Figure S2b).

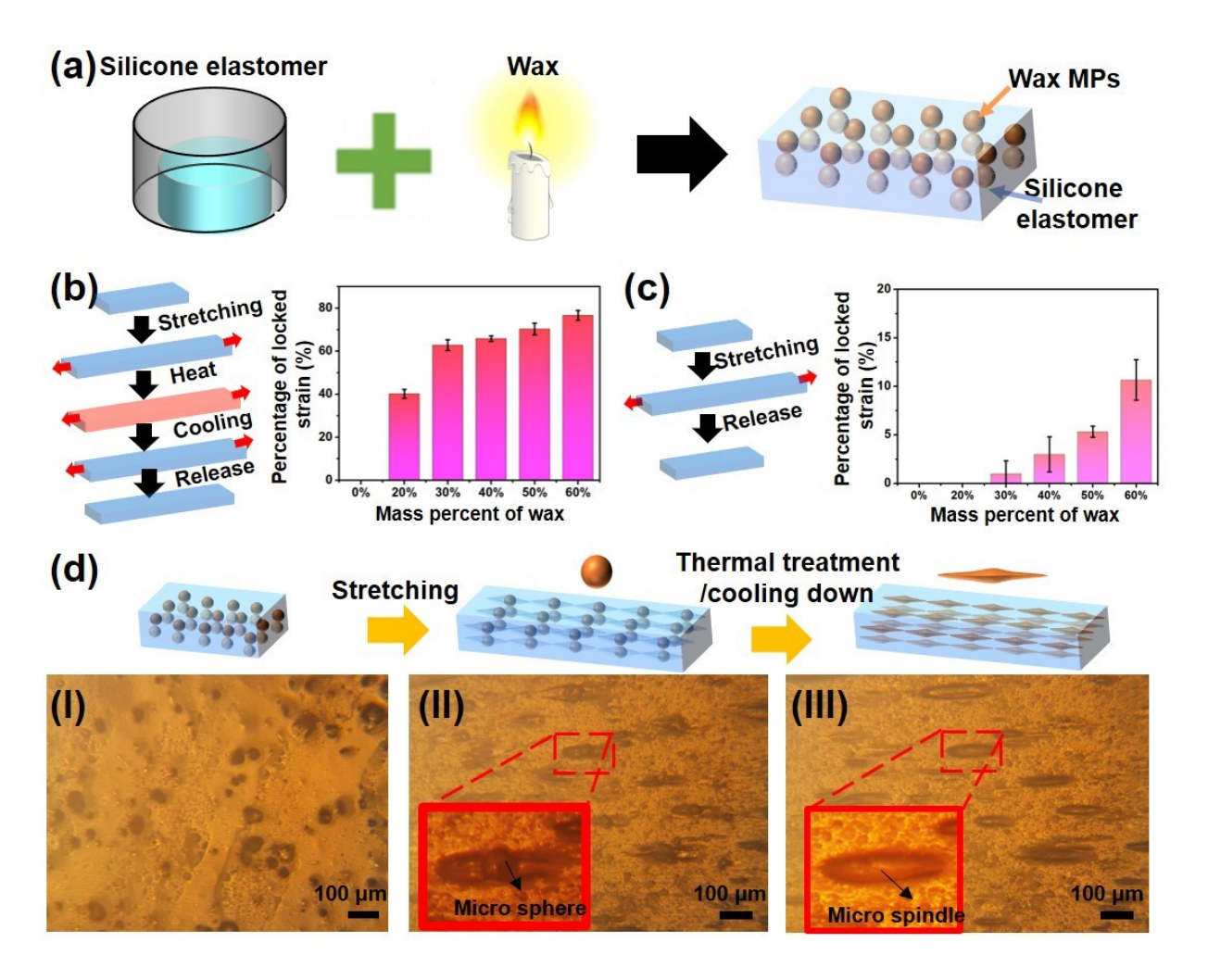


**Figure 2.** (a) Schematic of fabricating W-silicone composite (b) Schematic of residual strain in W-silicone strips and their correlation with the mass ratio of the wax. (c) Schematic of elasticity test of W-silicone and relationship between the mass ratio of wax and residual strain. (d) Schematic and optical images showing morphology evolving of the wax microstructures during the programming process. To better observe their morphology, a sample with a low wax loading (5 wt%) was used.

To probe the origin of the residual strain caused by the thermal patterning, we investigated the evolving of morphology changes of the wax microstructures by optical microscopy. As shown in Figure 2d-I, due to the phase separation, 30-70 µm wax MPs are physically dispersed in the matrix of silicone elastomer. Because in a solid state the wax is much stiffer than the elastomer, when the W-silicone is stretched, the wax MPs are detached from the interface of the elastomer and the wax MPs, leaving empty gaps between the wax MPs and elastomer cavities (Figure 2d-II). Meanwhile,

the elastomer cavity is deformed to a spindle shape. When heated, the melt wax MPs fill in the gaps and form the same spindle shape as the cavity in the elastomer. After cooled down, micro wax spindles are fixed (Figure 2d-III) and resist full recovery of the W-silicone strips to the original shape after the applied stress is removed, thereby leading to the residual strain. When reheated, the wax micro spindles become liquid with a greatly decreased mechanical property, thus the residual strain in the W-silicone is erased. This interesting and novel 3D shape changing mechanism in this W-silicone composite lays solid foundation for fabricating complex 3D structures with reprogramming and reconfiguration capabilities.

To program complex 3D shapes, it is necessary to spatially control the residual strain with anisotropic distribution. To do that, local thermal treatment was applied to the stretched W-silicone sheets. A preheated alumina plate was used as a heating source to apply thermal patterns on the surface of a W-silicone sheet pre-stretched with 100% strain. The vertical anisotropic residual strain was generated by changing thermal exposure duration (Figure S3). A short duration, e.g. 2 seconds, only melts the wax that is close to the heat source in the thickness direction due to a temperature gradient, therefore creating vertical anisotropic residual strain (Figure 3a). The domains closer to the thermally exposed surface of the W-silicone sheet recover less than those farther, which makes the W-silicone sheet curve from the directly exposed surface to the non-exposed one. Depending on the exposure areas, the sheets were either bent (Figure 3b) or folded (Figure 3c). If both sides of the W-silicone sheets were thermally patterned, more complex structures resulting from bidirectional bending or folding were achieved (Figure 3d and 3e).

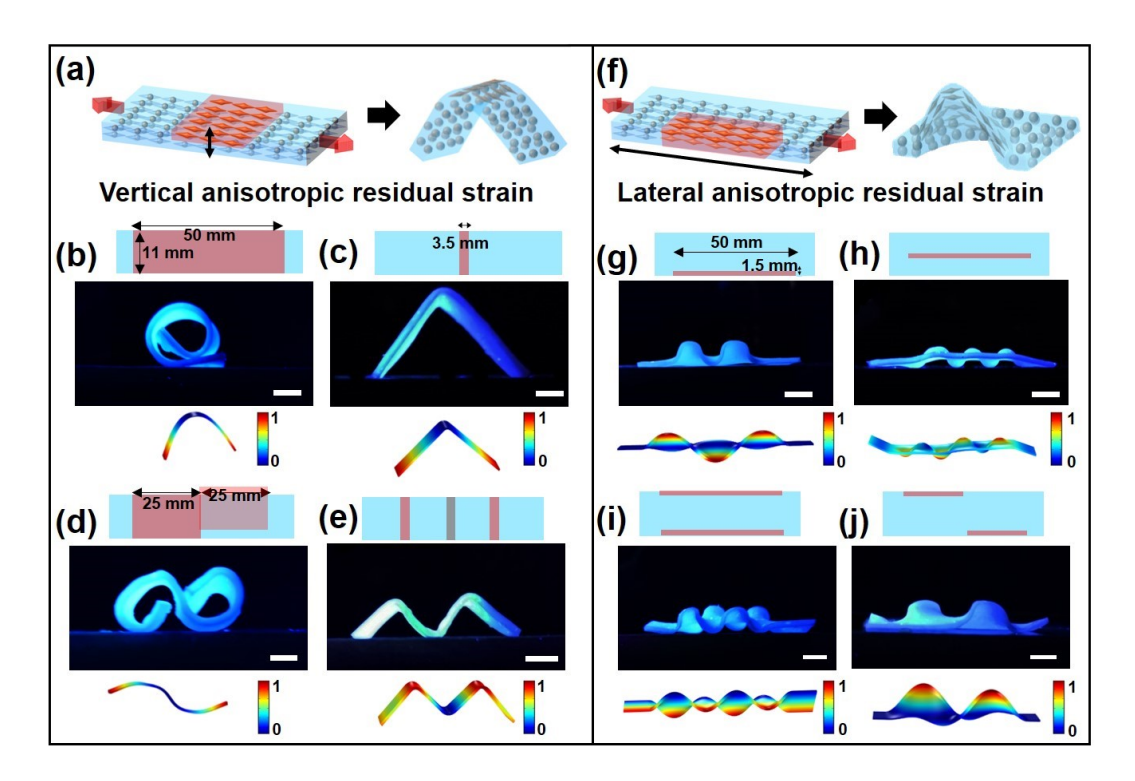


**Figure 3.** (a) Schematic of creating vertical anisotropic residual strain in W-silicone sheets (width: 11 mm, length: 60 mm, thickness: 1 mm). (b)-(c) Photographs and FEA simulation results of bent (b) and folded (c) W-silicone sheets. (d)-(e) Photograph and FEA simulation results of W-silicone 3D shapes caused by bidirectional bending (d) and folding (e). Rectangle area indicated as red represents a thermally exposed domain on the top side of a W-silicone sheet. Rectangle area indicated as grey is a thermally exposed domain on the bottom side of a W-silicone sheet. (f) Schematic of lateral anisotropic residual strain created in W-silicone sheets. (g-j) Photographs and FEA simulation results of various W-silicone 3D structures caused by buckling. Scale bars in all photographs are 5 mm. The color bars in FEA results represent normalized displacement of W-silicone sheets.

If the exposure time increases to 4 s, the exposed areas show uniform residual strain, but non-exposed ones show full elasticity. This residual strain anisotropy in the lateral direction creates in-plane buckling action (Figure 3f). By controlling the size and position of the exposure areas the W-silicone sheets were buckled into different types of wave-like shapes (Figure 3g-3j and Figure S4). Formation of these 3D structures was predicted by using the finite element analysis (FEA). The predicted 3D structures with corresponding displacement programs are shown below each example. The FEA simulation results agreed well with the experimental ones, suggesting the

possibility of using computational modeling to design the shape-morphed structures from the W-silicone sheets. These programmed 3D structures were erasable for reprogramming purpose. Figure S5 and Movie S1 show the recover process of a 3D structure to its original planar shape by hotplate heating. It should be noted that all the shape-morphing examples shown in Figure 3 were from the same W-silicone sheet, suggesting the versatility of the W-silicone composites for assembling different 3D structures. All the 3D structures shown in Figure 3 were realized by applying uniaxial strain. If biaxial strain is applied to the W-silicone sheet, more complex structures were obtained (Figure S6).

In addition to the aforementioned 3D structures that were fabricated by folding, bending and buckling, micro wrinkles were also realized on the surface of the W-silicone sheets. An effective method of fabricating wrinkles on a solid surface is to deposit a thin film on a stretched elastomer. 38-39 To form wrinkles, the deposited thin film should be more rigid and much thinner than the elastomer substrate. Thus, after the elastomer is released, the elastomer recovers to its original size, imparting compressive force to the deposited thin film to form micro or nano sinusoidal wrinkles. In this work, the key challenge of fabricating wrinkles on the W-silicone sheets is to develop a method that can form a relatively rigid and thin layer on the same prestretched W-silicone sheet. Herein, we employed low-power CO<sub>2</sub> laser writing to directly form a thin W-silicone layer that is more rigid than the underneath one due to the same mechanism explained previously (Figure 4a). The low-power CO<sub>2</sub> laser serves as a heating source to locally melt wax MPs in the W-silicone sheet. The result shows that it does not ablate or damage the structure of the elastomer matrix as shown in Figure S7. After the W-silicone sheet was relaxed from the applied tensile stress, the thin layer was buckled into micro wrinkle (Figure 4b), which was validated by the FEA simulation (Figure 4c). The first advantage of using the direct laser

writing as the thermal patterning technique arises from its generated transient heat on the exposed surface, 40-41 which limits thermal diffusion in both lateral and vertical directions of the W-silicone sheet. Thus, it is beneficial to form a very thin W-silicone layer with reasonable pattern resolution. Otherwise, if the thickness of the thermally affected layer is too large, bending rather than wrinkling would be realized as shown in Figure 3b. Second, the direct laser writing is digitally controlled with a high processing rate and design freedom.<sup>42</sup> Thus, complex 2D patterns can be directly written. As shown in Figure 4d, a cartoon Figure "Pikachu" was written on the W-silicone sheet by a CO<sub>2</sub> laser. This wrinkled pattern can be erased by removing residual strain locked in the laser exposed areas. Upon heating, the pattern gradually disappeared as shown in Figure S8 and Movie S2. Then the same W-silicone sheet was used to write another carton figure such as "Totoro" (Figure 4e). This reversibility makes the W-silicone a rewritable "paper". Compared to previously reported rewritable papers, our W-silicone based one possesses several advantages. For instance, many of the reported rewritable papers require complicated fabrication processes, 43 are volatile, 44 or need ultraviolet light to erase the information.<sup>45</sup> In contrast, the information can be directly written in our W-silicone rewritable "paper" by one step laser scribing. Moreover, it is non-volatile, thus requiring no additional energy input to keep the information.

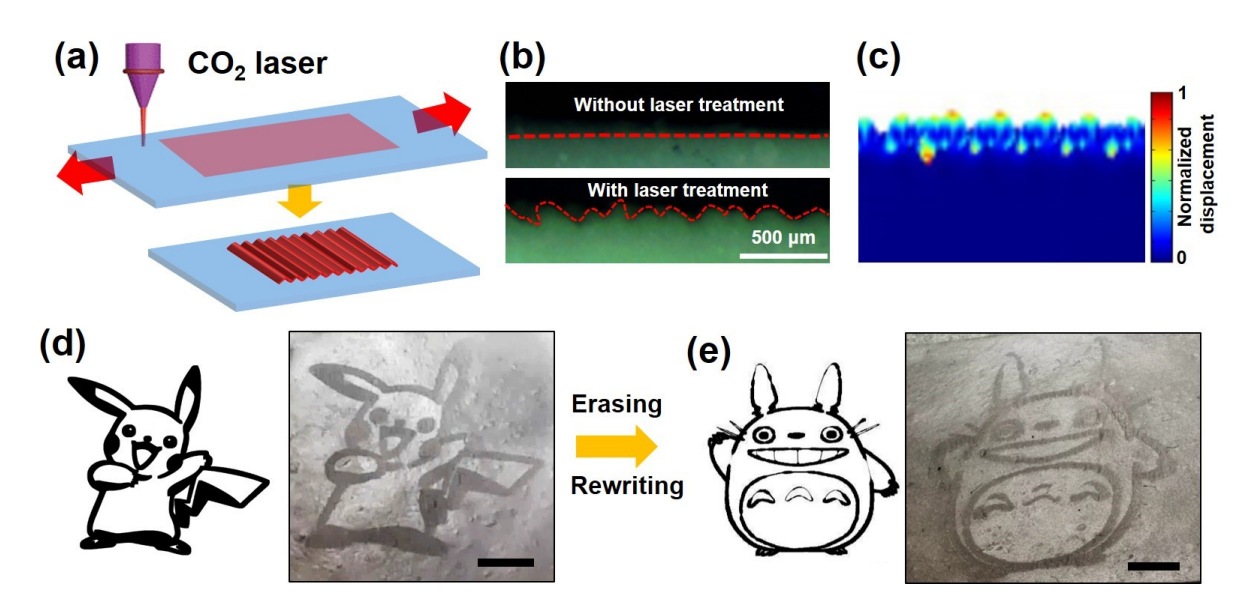


**Figure 4.** (a) Schematic of using CO<sub>2</sub> laser to thermally pattern a pre-stretched W-silicone sheet for fabricating surface wrinkles. Optical photographs (b) and FEA result (c) showing wrinkle structures on surface of a W-silicone sheet. (d)-(e) Photographs of "Pikachu" (d) and "Totoro" (e) patterns on surface of a W-silicone sheet. Scale bars in (d) and (e) are 1 cm.

3D structures showing shape reconfiguration for actuation are useful for practical applications. Herein, we demonstrate such a function of 3D structures fabricated from W-silicone composites by integrating them into a pneumatic system. Fabrication of the pneumatic W-silicone actuator is schematically represented in Figure S9 and described in the experimental section. To better observe the structures of the air chambers embedded in the W-silicone sheets, their walls were painted as red. The as-prepared pneumatic W-silicone actuator was composed of three petals (Figure 5a). When it was pressurized, the chambers were inflated with the expansion occurring in the most compliant (the thinnest) regions, <sup>46-47</sup> forming a bump in each petal (Figure 5b). The geometry of the actuator was programmed by the thermal patterning. As a simple demonstration, the petals were stretched along the axil (Figure 5c) and thermally patterned to generate anisotropic residual strain in the thickness direction of each petal. After released, each petal formed a 3D flower bud shape (Figure 5d). When pressurized, this unopened flower bud opened the petals due

to the inflation of the air chambers. Due to a large elasticity, the shape was recovered after it was deflated. The pneumatic system endowed the programmed 3D shape dynamic feature for shape reconfiguration. Then the programmed 3D shape was erased and reprogrammed by stretching the recovered sheet along the direction that was vertical to axil (Figure 5e). After the thermal patterning, each petal was curved in the direction perpendicular to the axil (Figure 5f). When pressurized, these curved petals were reconfigured differently as shown in Figure 5f. With these controllable and reversible motions, the pneumatic actuators were used as grippers to deliver plastic foam cargos. As represented in Figure 5g and Movies S3, when the actuator was inflated, the curved petals opened and then grabbed the cargo upon the deflation. When the cargo was transported to the destination site, the actuator was inflated to release the cargo. When the petals are programmed in the way as shown in Figure 5e, each petal individually grabbed one cargo (Figure S10 and Movie S3). The shape reprogramming and reconfiguration would pave a new route to fabricating multifunctional devices and robots.

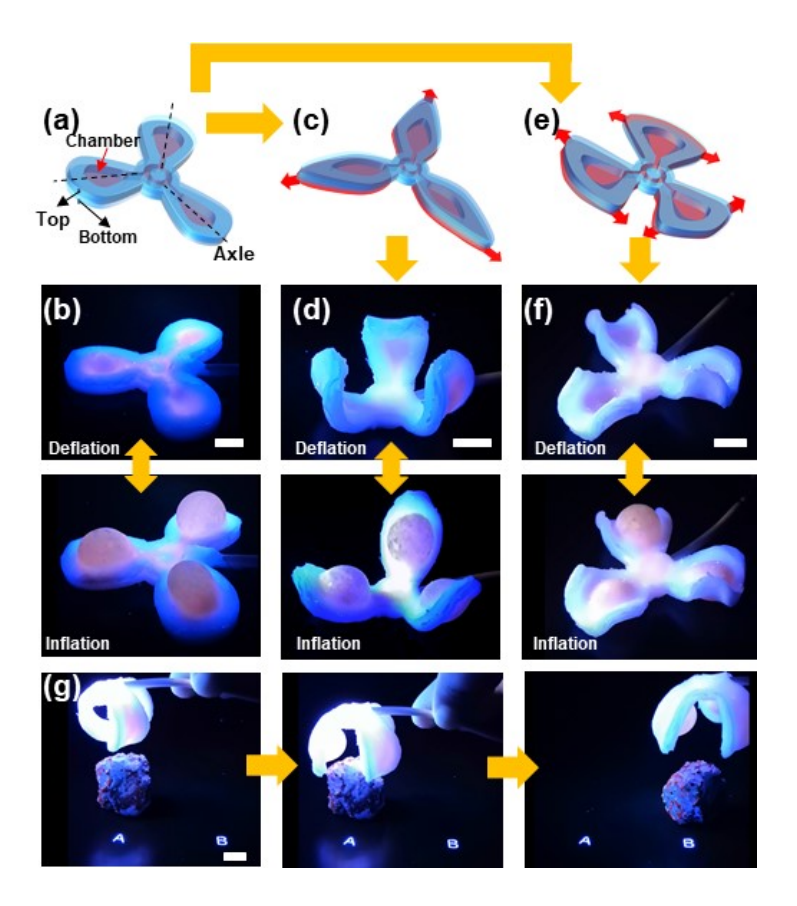


**Figure 5.** (a) Schematic of pneumatic actuators fabricated by programming W-silicone composites. The top wall (1 cm) is thinner than bottom wall (1.5 cm). (b) Photographs showing actuation upon inflation and deflation. (c)-(f) Schematic of programming shapes of pneumatic actuators (c), (e) and their corresponding actuation (d), (f) upon inflation and deflation. (g) Photographs of a programmed pneumatic actuator that cooperatively grabs a cargo and deliver it to a destination site. Scale bars in (b), (d), (f)-(g) are 1 cm.

Finally, the method we presented here for fabricating reprogrammable elastic composite is a transformative one, which is not limited by using wax as the phase change material and silicone elastomer as the matrix. Other types of phase change MPs and elastic materials are also suitable for building up the reprogrammable composite sheets. For instance, the PCL MPs with melting point of 60 °C and tough polyacrylamide (PAAm) hydrogel with high elasticity<sup>48</sup> were also adopted as phase change MPs and elastic matrix to constitute the reprogrammable composite sheets. To demonstrate this, we fabricated reprogrammable PCL-elastomer composite sheets and PCL-hydrogel composite sheets. The fabrication process is schematically represented in Figure 6a

and described in the experimental section. The PCL MPs with size of 10-30 µm (Figure S11) were firstly fabricated by dispersing melted PCL in polyvinyl alcohol (PVA) solution. Then the resulting PCL MPs were mixed with silicone or hydrogel precursor solutions to obtain composite sheets. To distinguish these two types of composite sheets, different colored PCL MPs (Figure S12) were used to fabricate PCL-silicone composite sheet (green) and PCL-hydrogel composite (pink). These two types of composite sheets possess the same programmability as the W-silicone has. By using the abovementioned thermal patterning method, different 3D shapes can be achieved in the same PCL-silicone composite sheet (Figure 6b) and PCL-hydrogel composite sheet (Figure 6c).

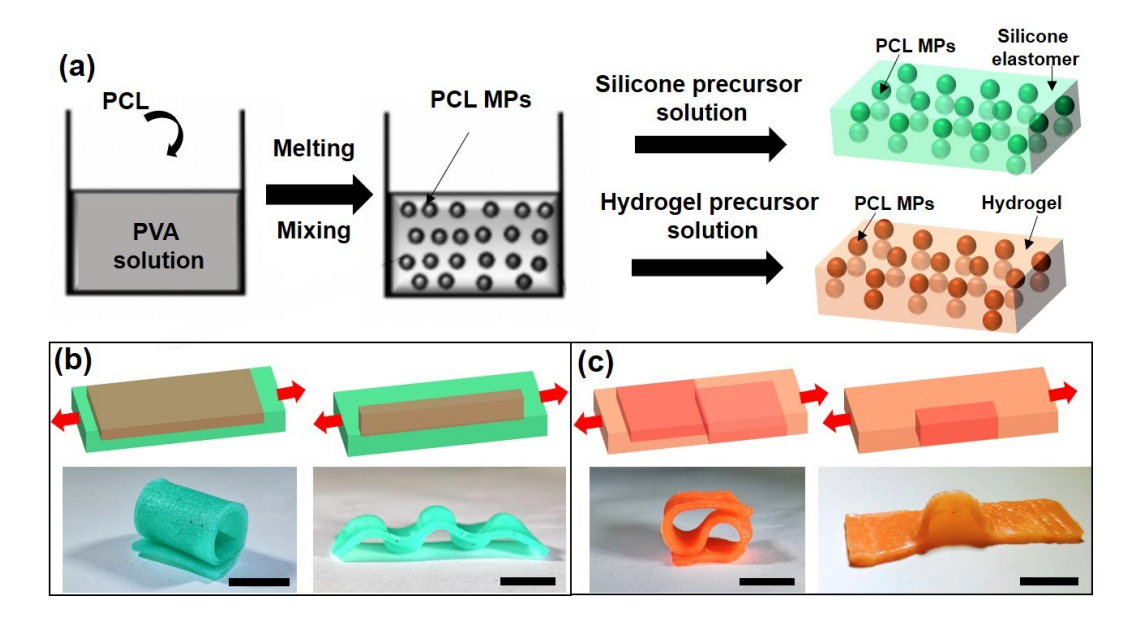


**Figure 6.** (a) Schematic of fabricating PCL-elastomer composite and PCL-hydrogel composite. (b) Photographs of shape programming of PCL-elastomer composite. (c) Photographs of shape programming of PCL-hydrogel composite. Scale bars in (b) and (c) are 1 cm.

# **CONCLUSIONS**

In summary, we developed a novel reprogrammable shape-morphing material by embedding phase changing MPs (such as wax MPs and PCL MPs) in elastic polymeric matrix. By a simple thermal patterning process on the pre-stretched composite sheets, anisotropic residual strain was created due to the phase change of the phase change MPs after the sheets were relaxed. The residual strain

triggers the shape transformation from 2D sheets to 3D structures. The thermal patterning technique was easy and robust, involving no spatially resolved mechanical forces or chemical treatments. Multiple types of shape-changing behaviors, including bending, folding, buckling, and wrinkling were demonstrated on the composite sheets. Because the phase change process is reversible, the programmed 3D structures can be erased and reprogrammed to different 3D geometries. Such reprogrammed elastic composites showed potential in promising applications as a rewritable "paper" and a reconfigurable pneumatic actuator. Finally, the method we presented here is transformative and can be suitable for a wide range of material systems, which will show substantial progress in making multifunctional devices or robotic systems for widespread applications.

## **METHODS**

**Fabrication of wax-silicone composites**. First, part A and part B of commercial silicone solution (Ecoflex 00-30) were individually mixed with liquid wax (Mainstays white unscented pillar candle) on a hotplate with a set temperature of 100 °C to obtain part A/wax and part B/wax composites. After cooled down, the part A/wax and part B/wax were mixed with a volume ratio of 1:1 at room temperature. The mixtures were then poured into a mold and cured to form wax-silicone (W-silicone) composite at room temperature for 4 h.

**Fabrication of PCL-silicone and PCL-hydrogel composites**. First, 1 g polycaprolactone (PCL) filament was mixed homogeneously with 10 ml polyvinyl alcohol (PVA) aqueous solution (15 wt%) on a hotplate with a set temperature of 100 °C. Due to the phase separation, PCL MPs would be formed and dispersed in PVA solution. Then the PCL MPs were purified by a centrifuge in 100 ml water at a speed of 2000 rpm for at least 3 times. To fabricate PCL-silicone composites,

part A and part B of commercial silicone solution (Ecoflex 00-30) were firstly mixed with a volume ratio of 1:1 at room temperature. Then the mixed silicone solution (0.7 g) were mixed with PCL MPs (0.3 g). Finally, the mixture was poured into a mold and cured to form PCL-silicone composites. To fabricate PCL- hydrogel composites, 0.3 g ml PCL MPs were mixed with 0.7 g of a polyacrylamide (PAAm) hydrogel aqueous precursor solution (12 wt% acrylamide, 2 wt% sodium alginate, 2 wt % PVA, 0.024 wt% methylene-N,N'-bis(acrylamide), 0.26 wt% calcium sulphate, 0.03 wt N,N,N',N'-tetramethylethylenediamine and 0.043 wt% ammonium peroxodisulfate). Then the mixture was poured into a mold and cured to form PCL-hydrogel composites.

Fabrication of a pneumatic actuator. Negative mold A (with air chamber) and mold B (without air chamber) were designed by Solidworks. A 3D printer printed the designed molds. Then part A/wax and part B/wax composites were poured into these two molds and cured at room temperature for 4 h, respectively. After they were fully cured, W-silicone layer A (from mold A) and W-silicone layer B (from mold B) were released from the molds. A thin layer of wax/silicone mixture was coated on W-silicone layer B for bonding W-silicone layer A at room temperature for 4 h. To connect the air chambers in the pneumatic actuator to an external gas source, polyurethane tubing was inserted. A syringe was then connected to the polyurethane tubing to pressurize the air into the chambers.

**3D shape programming**. The composite sheets were fixed in a home-made stretcher and stretched to a strain of 100%. Then we used a preheated aluminum plate and CO<sub>2</sub> laser writing to do the thermal patterning. The aluminum plate was firstly pre-heated to 100 °C on a hotplate and then placed on a stretched wax-silicone sheet for certain durations (2-4 seconds). After the composite sheet were cooled down, the applied external stress was removed to form 3D structures. In the case

of the CO<sub>2</sub> laser patterning, the power of CO<sub>2</sub> laser was set to 7.2 W. The desired patterns were loaded onto the software for controlling the movement of the CO<sub>2</sub> laser beam. The programmed 3D structures could recover to the original planar shape by heating on a hotplate or a blow drier. **Characterization**. Optical images of W-silicone composites and PCL MPs were taken using a microscope (AmScope). Graphical analysis was done by the AmScope software. It should be noted that, in order to clearly observe the structures of W-silicone, we fabricated a W-silicone composite with 5 wt% wax. Tensile testing of the wax-silicone composites was conducted on a Mark-10 ESM303 tensile tester. The videos and photographs of 3D structures were taken by a smart phone under UV light.

FEA simulation. The FEA simulations were performed in commercial software COMSOL-Multiphysics. The wax-silicone was assumed to be linearly elastic isotropic materials. Young's modulus of the wax-silicone composites with 30 wt% wax was set to 81.8 kPa based on the measurement results derived from the curves of tensile testing (Figure S13). Its Poisson's ratio and mass density were set to 0.23 and 1200 kg/m³, respectively. In the simulation, a pre-strain of -0.5 was applied to non-exposed regions and a pre-strain of -0.2 was applied to thermally exposed regions.

#### ASSOCIATED CONTENT

## **Supporting Information**

The Supporting Information is available free of charge on the ACS Publications website. Detailed descriptions of optical images of W-silicone composite with different residual strains, thermal pattering process, additional optical images of assembled 3D architectures, erasing process on W-elastomer rewritable paper, fabrication of pneumatic actuator, process of individual grabbing

actuation, optical images of PCL microparticles and stress-strain curves of W-silicone composite

(PDF)

Recovering process of a buckled W-silicone sheet (AVI)

Erasing process on W-silicone rewritable paper (AVI)

Process of individual or cooperative grabbing actuation (AVI)

**Corresponding Authors** 

\*E-mail: huangg@missouri.edu (G.H.).

\*E-mail: LinJian@missouri.edu (J.L.).

**ORCID** 

Jian Lin: 0000-0002-4675-2529

Notes

The authors declare no competing financial interest.

**ACKNOWLEDGMENTS** 

J.L. thanks the financial support from National Science Foundation (Award number: 1825352)

with Program Manager Dr. Khershed Cooper and Unite States Department of Agriculture (Award

number: 2018-67017-27880). G.H. acknowledges the support by the Air Force Office of Scientific

Research under Grant No. AF 9550-18-1-0342 with Program Manager Dr. Byung-Lip (Les) Lee.

20

#### REFERENCES

- (1) Le, X.; Lu, W.; Zhang, J.; Chen, T. Recent Progress in Biomimetic Anisotropic Hydrogel Actuators. *Adv. Sci.* **2018**, 1801584.
- (2) Ma, M.; Guo, L.; Anderson, D. G.; Langer, R. Bio-inspired Polymer Composite Actuator and Generator Driven by Water Gradients. *Science* **2013**, *339* (6116), 186-189.
- (3) Zhang, Y. S.; Khademhosseini, A. Advances in Engineering Hydrogels. *Science* **2017**, *356* (6337), eaaf3627.
- (4) Ionov, L. Biomimetic Hydrogel- Based Actuating Systems. *Adv. Funct. Mater.* **2013**, *23* (36), 4555-4570.
- (5) Liu, Y.; Genzer, J.; Dickey, M. D. "2D or not 2D": Shape-programming Polymer Sheets. *Prog. Polym. Sci.* **2016**, *52*, 79-106.
- (6) Berndt, A. J.; Hwang, J.; Islam, M. D.; Sihn, A.; Urbas, A. M.; Ku, Z.; Lee, S. J.; Czaplewski, D. A.; Dong, M.; Shao, Q.; Wu, S.; Guo, Z.; Ryu, J. E. Poly(sulfur-random-(1,3-diisopropenylbenzene)) Based Mid-wavelength Infrared Polarizer: Optical Property Experimental and Theoretical Analysis. *Polymer* **2019**, *176*, 118-126.
- (7) Zhang, Y.; An, Y.; Wu, L.; Chen, H.; Li, Z.; Dou, H.; Murugadoss, V.; Fan, J.; Zhang, X.; Mai, X.; Guo, Z. Metal-free Energy Storage Systems: Combining Batteries with Capacitors Based on a Methylene Blue Functionalized Graphene Cathode. *J. Mater. Chem. A* **2019**, *7* (34), 19668-19675. (8) Oyefusi, A.; Chen, J. Reprogrammable Chemical 3D Shaping for Origami, Kirigami, and Reconfigurable Molding. *Angew. Chem. Int. Edit.* **2017**, *56* (28), 8250-8253.
- (9) Grimm, D.; Bufon, C. C. B.; Deneke, C.; Atkinson, P.; Thurmer, D. J.; Schaffel, F.; Gorantla, S.; Bachmatiuk, A.; Schmidt, O. G. Rolled-up Nanomembranes as Compact 3D Architectures for Field Effect Transistors and Fluidic Sensing Applications. *Nano Lett.* **2013**, *13* (1), 213-218.
- (10) Xu, S.; Yan, Z.; Jang, K. I.; Huang, W.; Fu, H. R.; Kim, J.; Wei, Z.; Flavin, M.; McCracken, J.; Wang, R.; Badea, A.; Liu, Y.; Xiao, D. Q.; Zhou, G. Y.; Lee, J.; Chung, H. U.; Cheng, H. Y.; Ren, W.; Banks, A.; Li, X. L.; Paik, U.; Nuzzo, R. G.; Huang, Y. G.; Zhang, Y. H.; Rogers, J. A. Assembly of Micro/nanomaterials into Complex, Three-dimensional Architectures by Compressive Buckling. *Science* **2015**, *347* (6218), 154-159.
- (11) Zhang, Y. H.; Yan, Z.; Nan, K. W.; Xiao, D. Q.; Liu, Y. H.; Luan, H. W.; Fu, H. R.; Wang, X. Z.; Yang, Q. L.; Wang, J. C.; Ren, W.; Si, H. Z.; Liu, F.; Yang, L. H.; Li, H. J.; Wang, J. T.; Guo, X. L.; Luo, H. Y.; Wang, L.; Huang, Y. G.; Rogers, J. A. A Mechanically Driven Form of Kirigami as a Route to 3D Mesostructures in Micro/nanomembranes. *Proc. Natl. Acad. Sci.* **2015**, *112* (38), 11757-11764.
- (12) Yan, Z.; Zhang, F.; Liu, F.; Han, M. D.; Ou, D. P.; Liu, Y. H.; Lin, Q.; Guo, X. L.; Fu, H. R.; Xie, Z. Q.; Gao, M. Y.; Huang, Y. M.; Kim, J.; Qiu, Y. T.; Nan, K. W.; Kim, J.; Gutruf, P.; Luo, H. Y.; Zhao, A.; Hwang, K. C.; Huang, Y. G.; Zhang, Y. H.; Rogers, J. A. Mechanical Assembly of Complex, 3D Mesostructures from Releasable Multilayers of Advanced Materials. *Sci. Adv.* **2016**, *2* (9), e1601014.
- (13) Han, M. D.; Wang, H. L.; Yang, Y. Y.; Liang, C. M.; Bai, W. B.; Yan, Z.; Li, H. B.; Xue, Y. G.; Wang, X. L.; Akar, B.; Zhao, H. B.; Luan, H. W.; Lim, J.; Kandela, I.; Ameer, G. A.; Zhang, Y. H.; Huang, Y. G.; Rogers, J. A. Three-dimensional Piezoelectric Polymer Microsystems for Vibrational Energy Harvesting, Robotic Interfaces and Biomedical Implants. *Nat. Electron* **2019**, *2* (1), 26-35.
- (14) Lee, W.; Liu, Y.; Lee, Y.; Sharma, B. K.; Shinde, S. M.; Kim, S. D.; Nan, K.; Yan, Z.; Han, M. D.; Huang, Y. G.; Zhang, Y. H.; Ahn, J. H.; Rogers, J. A. Two-dimensional Materials in

- Functional Three-dimensional Architectures with Applications in Photodetection and Imaging. *Nat. Commun.* **2018,** *9*, 1417.
- (15) Ling, Y.; Zhuang, X. T.; Xu, Z.; Xie, Y. C.; Zhu, X. Y.; Xu, Y. D.; Sun, B. H.; Lin, J.; Zhang, Y. H.; Yan, Z. Mechanically Assembled, Three-dimensional Hierarchical Structures of Cellular Graphene with Programmed Geometries and Outstanding Electromechanical Properties. *ACS Nano* **2018**, *12* (12), 12456-12463.
- (16) Yan, Z.; Han, M. D.; Shi, Y.; Badea, A.; Yang, Y. Y.; Kulkarni, A.; Hanson, E.; Kandel, M. E.; Wen, X. W.; Zhang, F.; Luo, Y. Y.; Lin, Q.; Zhang, H.; Guo, X. G.; Huang, Y. M.; Nan, K. W.; Jia, S.; Oraham, A. W.; Mevis, M. B.; Lim, J. M.; Guo, X. L.; Gao, M. Y.; Ryu, W.; Yu, K. J.; Nicolau, B. G.; Petronico, A.; Rubakhin, S. S.; Lou, J.; Ajayan, P. M.; Thornton, K.; Popescu, G.; Fang, D. N.; Sweedler, J. V.; Braun, P. V.; Zhang, H. X.; Nuzzo, R. G.; Huang, Y. G.; Zhang, Y. H.; Rogers, J. A. Three-dimensional Mesostructures as High-temperature Growth Templates, Electronic Cellular Scaffolds, and Self-propelled Microrobots. *Proc. Natl. Acad. Sci.* **2017**, *114* (45), 9455-9464.
- (17) McCracken, J. M.; Xu, S.; Badea, A.; Jang, K. I.; Yan, Z.; Wetzel, D. J.; Nan, K. W.; Lin, Q.; Han, M. D.; Anderson, M. A.; Lee, J. W.; Wei, Z. J.; Pharr, M.; Wang, R. H.; Su, J.; Rubakhin, S. S.; Sweedler, J. V.; Rogers, J. A.; Nuzzo, R. G. Deterministic Integration of Biological and Soft Materials onto 3D Microscale Cellular Frameworks. *Adv. Biosyst.* **2017**, *1* (9), 1700068.
- (18) Wang, X. J.; Guo, X. G.; Ye, J. L.; Zheng, N.; Kohli, P.; Cho, D. W.; Zhang, Y.; Xie, Z. Q.; Zhang, Q. H.; Luan, H. W.; Nan, K. W.; Kim, B. H.; Xu, Y. M.; Shan, X. W.; Bai, W. B.; Sun, R. J.; Wang, Z. Z.; Jang, H. Y.; Zhang, F.; Ma, Y. J.; Xu, Z.; Feng, X.; Xie, T.; Huang, Y. G.; Zhang, Y. H.; Rogers, J. A. Freestanding 3D Mesostructures, Functional Devices, and Shape-Programmable Systems Based on Mechanically Induced Assembly with Shape Memory Polymers. *Adv. Mater.* **2019**, *31* (2), 1805615.
- (19) Kempaiah, R.; Nie, Z. From Nature to Synthetic Systems: Shape Transformation in Soft Materials. *J. Mater. Chem. B* **2014**, *2* (17), 2357-2368.
- (20) Kim, J.; Hanna, J. A.; Byun, M.; Santangelo, C. D.; Hayward, R. C. Designing Responsive Buckled Surfaces by Halftone Gel Lithography. *Science* **2012**, *335* (6073), 1201-1205.
- (21) Jamal, M.; Zarafshar, A. M.; Gracias, D. H. Differentially Photo-crosslinked Polymers Enable Self-assembling Microfluidics. *Nat. Commun.* **2011,** *2*, 527.
- (22) Peng, X.; Liu, T.; Zhang, Q.; Shang, C.; Bai, Q. W.; Wang, H. Surface Patterning of Hydrogels for Programmable and Complex Shape Deformations by Ion Inkjet Printing. *Adv. Funt. Mater.* **2017**, *27* (33), 1701962.
- (23) Su, J.-W.; Tao, X.; Deng, H.; Zhang, C.; Jiang, S.; Lin, Y.; Lin, J. 4D Printing of a Self-morphing Polymer driven by a Swellable Guest Medium. *Soft Matter* **2018**, *14* (5), 765-772.
- (24) Gladman, A. S.; Matsumoto, E. A.; Nuzzo, R. G.; Mahadevan, L.; Lewis, J. A. Biomimetic 4D Printing. *Nat. Mater.* **2016**, *15* (4), 413-418.
- (25) Erb, R. M.; Sander, J. S.; Grisch, R.; Studart, A. R. Self-shaping Composites with Programmable Bioinspired Microstructures. *Nat. Commun.* **2013**, *4*, 1712.
- (26) Huang, H.-W.; Sakar, M. S.; Petruska, A. J.; Pané, S.; Nelson, B. J. Soft Micromachines with Programmable Motility and Morphology. *Nat. Commun.* **2016,** *7*, 12263.
- (27) Deng, H.; Zhang, C.; Su, J.-W.; Xie, Y.; Zhang, C.; Lin, J. Bioinspired Multi-responsive Soft Actuators Controlled by Laser Tailored Graphene Structures. *J. Mater. Chem. B* **2018**, *6* (34), 5415-5423.
- (28) Deng, H.; Dong, Y.; Zhang, C.; Xie, Y.; Zhang, C.; Lin, J. An Instant Responsive Polymer Driven by Anisotropy of Crystal Phases. *Mater. Horiz.* **2018**, *5* (1), 99-107.

- (29) Deng, H.; Dong, Y.; Su, J.-W.; Zhang, C.; Xie, Y.; Zhang, C.; Maschmann, M. R.; Lin, Y.; Lin, J. Bioinspired Programmable Polymer Gel Controlled by Swellable Guest Medium. *ACS Appl. Mater. Interfaces* **2017**, *9* (36), 30900-30908.
- (30) Zhang, C.; Su, J.-W.; Deng, H.; Xie, Y.; Yan, Z.; Lin, J. Reversible Self-Assembly of 3D Architectures Actuated by Responsive Polymers. *ACS Appl. Mater. Interfaces* **2017**, *9* (47), 41505-41511.
- (31) Meng, H.; Li, G. A Review of Stimuli-responsive Shape Memory Polymer Composites. *Polymer* **2013**, *54* (9), 2199-2221.
- (32) Zhao, Q.; Qi, H. J.; Xie, T. Recent Progress in Shape Memory Polymer: New Behavior, Enabling Materials, and Mechanistic Understanding. *Prog. Polym. Sci.* **2015**, *49*, 79-120.
- (33) Zhao, Q.; Zou, W.; Luo, Y.; Xie, T. Shape Memory Polymer Network with Thermally Distinct Elasticity and Plasticity. *Sci. Adv.* **2016**, *2* (1), e1501297.
- (34) Kohlmeyer, R. R.; Buskohl, P. R.; Deneault, J. R.; Durstock, M. F.; Vaia, R. A.; Chen, J. Shape-reprogrammable Polymers: Encoding, Erasing, and Reencoding. *Adv. Mater.* **2014**, *26* (48), 8114-8119.
- (35) Yang, Y.; Terentjev, E. M.; Wei, Y.; Ji, Y. Solvent-assisted Programming of Flat Polymer Sheets into Reconfigurable and Self-healing 3D Structures. *Nat. Commun.* **2018**, *9* (1), 1906.
- (36) Owuor, P. S.; Chaudhary, V.; Woellner, C. F.; Sharma, V.; Ramanujan, R.; Stender, A. S.; Soto, M.; Ozden, S.; Barrera, E. V.; Vajtai, R. High Stiffness Polymer Composite with Tunable Transparency. *Mater. Today* **2018**, *21* (5), 475-482.
- (37) Su, J.-W.; Wang, J.; Zheng, Y.; Jiang, S.; Lin, J. Mechanically Guided Assembly of Monolithic Three-Dimensional Structures from Elastomer Composites. *ACS Appl. Mater. Interfaces* **2018**, *10* (51), 44716-44721.
- (38) Genzer, J.; Groenewold, J. Soft Matter with Hard Skin: From Skin Wrinkles to Templating and Material Characterization. *Soft Matter* **2006**, *2* (4), 310-323.
- (39) Efimenko, K.; Rackaitis, M.; Manias, E.; Vaziri, A.; Mahadevan, L.; Genzer, J. Nested Self-Similar Wrinkling Patterns in Skins. *Nat. Mater.* **2005**, *4* (4), 293-297.
- (40) Deng, H.; Zhang, C.; Xie, Y.; Tumlin, T.; Giri, L.; Karna, S. P.; Lin, J. Laser Induced MoS 2/carbon Hybrids for Hydrogen Evolution Reaction Catalysts. *J. Mater. Chem. A* **2016**, *4* (18), 6824-6830.
- (41) Lin, J.; Peng, Z.; Liu, Y.; Ruiz-Zepeda, F.; Ye, R.; Samuel, E. L.; Yacaman, M. J.; Yakobson, B. I.; Tour, J. M. Laser-induced Porous Graphene Films from Commercial Polymers. *Nat. Commun.* **2014**, *5*, 5714.
- (42) Chyan, Y.; Cohen, J.; Wang, W.; Zhang, C.; Tour, J. M. Graphene Art. ACS Applied Nano Materials 2019, 2(5), 3007-3011
- (43) Sheng, L.; Li, M.; Zhu, S.; Li, H.; Xi, G.; Li, Y.-G.; Wang, Y.; Li, Q.; Liang, S.; Zhong, K. Hydrochromic Molecular Switches for Water-jet Rewritable Paper. *Nat. Commun.* **2014**, *5*, 3044.
- (44) Wang, W.; Feng, J.; Ye, Y.; Lyu, F.; Liu, Y.-s.; Guo, J.; Yin, Y. Photocatalytic Color Switching of Transition Metal Hexacyanometalate Nanoparticles for High-performance Light-printable Rewritable Paper. *Nano Lett.* **2017**, *17* (2), 755-761.
- (45) Wang, W.; Ye, Y.; Feng, J.; Chi, M.; Guo, J.; Yin, Y. Enhanced Photoreversible Color Switching of Redox Dyes Catalyzed by Barium- Doped TiO2 Nanocrystals. *Angew. Chem. Int. Edit.* **2015**, *54* (4), 1321-1326.
- (46) Martinez, R. V.; Branch, J. L.; Fish, C. R.; Jin, L.; Shepherd, R. F.; Nunes, R. M.; Suo, Z.; Whitesides, G. M. Robotic Tentacles with Three-dimensional Mobility Based on Flexible Elastomers. *Adv. Mater.* **2013**, *25* (2), 205-212.

- (47) Martinez, R. V.; Fish, C. R.; Chen, X.; Whitesides, G. M. Elastomeric Origami: Programmable Paper- elastomer Composites as Pneumatic Actuators. *Adv. Funt. Mater.* **2012**, *22* (7), 1376-1384.
- (48) Yuk, H.; Zhang, T.; Lin, S.; Parada, G. A.; Zhao, X. Tough Bonding of Hydrogels to Diverse Non-porous Surfaces. *Nat. Mater.* **2016**, *15* (2), 190-196.

